Original Article

MOLECULAR METABOLISM

Hindbrain REV-ERB nuclear receptors regulate sensitivity to diet-induced obesity and brown adipose tissue pathophysiology

Lauren N. Woodie[1], Lily C. Melink[1], Ahren J. Alberto[1], Michelle Burrows[1], Samantha M. Fortin[2], Calvin C. Chan[1,2], Matthew R. Hayes[1,2], Mitchell A. Lazar[1,*]

ABSTRACT

Objective: The dorsal vagal complex (DVC) of the hindbrain is a major point of integration for central and peripheral signals that regulate a wide variety of metabolic functions to maintain energy balance. The REV-ERB nuclear receptors are important modulators of molecular metabolism, but their role in the DVC has yet to be established.

Methods: Male REV-ERBα/β floxed mice received stereotaxic injections of a Cre expressing virus to the DVC to create the DVC REV-ERBα/β double knockout (DVC RDKO). Control littermates received stereotaxic injections to the DVC of a green fluorescent protein expressing virus. Animals were maintained on a normal chow diet or a 60% high-fat diet to observe the metabolic phenotype arising from DVC RDKO under healthy and metabolically stressed conditions.

Results: DVC RDKO animals on high-fat diet exhibited increased weight gain compared to control animals maintained on the same diet. Increased weight gain in DVC RDKO animals was associated with decreased basal metabolic rate and dampened signature of brown adipose tissue activity. RDKO decreased gene expression of calcitonin receptor in the DVC and tyrosine hydroxylase in the brown adipose tissue.

Conclusions: These results suggest a previously unappreciated role of REV-ERB nuclear receptors in the DVC for maintaining energy balance and metabolic rate potentially through indirect sympathetic outflow to the brown adipose tissue.

Keywords REV-ERBα/β; Dorsal vagal complex; Diet-induced obesity; Brown adipose tissue; Metabolic rate

1. INTRODUCTION

Obesity is a major public health issue with myriad treatment options but a lack of highly effective, long-term therapies [1,2]. Although development of obesity is complex and multifactorial, obesity is a disease of energy balance dysregulation in the brain [3,4]. While the neural controls of energy balance are distributed across the brain [5,6], the dorsal vagal complex (DVC) of the hindbrain is a major integrator of peripheral and central metabolic signals [5,7]. The DVC is comprised of the area postrema (AP), nucleus of the solitary tract (NTS), and the dorsal motor nucleus of ten (DMX). The AP and NTS receive afferent information regarding macronutrient composition of meals and gastric distention while the DMX sends efferent signals to peripheral organs ranging from the heart to the reproductive tract via the vagus nerve [8—11]. Thus, the DVC as a collective structure is an integral gatekeeper of regulatory flow between central and peripheral sources of homeostatic energy signals.

Due to this, the DVC has garnered attention as a central area of action for weight management pharmaceuticals. Metabolic signals such as glucagon-like peptide, melanocortin 3 and 4, leptin, insulin, and calcitonin are highly expressed in the DVC and are targets of interest for obesity therapeutics [7,12—16]. However, the molecular mechanisms underpinning DVC control of energy balance remains poorly understood.

REV-ERB α and β nuclear receptors are important for maintaining tissue-specific molecular metabolism [17]. They are transcriptional repressors that constitute a critical negative arm of the mammalian circadian clock [17] and directly repress thousands of genes [18—20]. In peripheral tissues, REV-ERBs modulate lipid and glucose handling and their depletion produces metabolic maladies such as hepatosteatosis, dyslipidemia, and impaired glucose and insulin tolerance [18,21—23]. The central roles of REV-ERBs are primarily behavioral such that loss of expression in the whole body or brain induces disturbances in sleep, memory, and social behaviors [24—26]. However, in specific groups of neurons or brain areas REV-ERBs control centrally mediated metabolic functions and it is unknown whether the DVC is one of these areas [23,27,28].

Therefore, a critical unmet need of the field is to determine how REV-ERBs function in the DVC. Therefore, we knocked out REV-ERBα/β in the DVC (DVC RDKO) of male mice to determine the effect of RDKO on

[1]Institute for Diabetes, Obesity, and Metabolism, and Division of Endocrinology, Diabetes, and Metabolism, Department of Medicine, Perelman School of Medicine at the University of Pennsylvania, Philadelphia, PA 19104, USA [2]Department of Psychiatry, Perelman School of Medicine at the University of Pennsylvania, Philadelphia, PA 19104, USA

*Corresponding author. E-mail: lazar@pennmedicine.upenn.edu (M.A. Lazar).

Received August 26, 2023 • Revision received December 8, 2023 • Accepted December 20, 2023 • Available online 23 December 2023

https://doi.org/10.1016/j.molmet.2023.101861

metabolic homeostasis. Here we report that DVC RDKO exacerbates high-fat diet-induced obesity (DIO) by decreasing basal metabolic rate. Our results suggest this may be due to decreased brown adipose tissue (BAT) activity arising potentially from indirect DVC control of sympathetic nervous system (SNS) outflow.

2. MATERIALS AND METHODS

2.1. Animals and diet

All animal work was approved by the University of Pennsylvania Perelman School of Medicine Institutional Animal Care and Use Committee (IACUC protocol number 804747 issued to Mitchell Lazar). Male *Nr1d1*$^{fl/fl}$/*Nr1d2*$^{fl/fl}$ [29] mice were maintained on a C57Bl6/J background (Jackson Labs, Stock 008661). Mice were bred and maintained at 20–22 °C on a 12:12 h light:dark cycle with *ad libitum* access to food and water unless otherwise noted. The normal chow diet (NCD, LabDiet, 5010) consisted of 12.7% kcal fat, 28.7% kcal protein, and 58.5% kcal carbohydrates. The high-fat diet (HFD, Research Diets, D12492) consisted of 60% kcal fat from lard and soybean oil, 20% kcal protein, and 20% kcal carbohydrates with 5.24 kcal/g. Surgical procedures were performed on 6–8-week-old male littermates. Sacrifice and tissue collection were performed 7 h after lights on to capture the peak time of REV-ERB expression [28].

2.2. Stereotaxic surgery

To perform injections, animals were anesthetized with isoflurane and secured into the stereotaxis (Stoelting Instruments, 51730U). A surgical plane of anesthesia was confirmed by toe pinch. Depilatory cream was used to remove animals' fur on the dorsal aspect of the head and neck before alternating EtOH and betadine swabs and application of a surgical drape. Subcutaneous, pre-operative analgesic (5 mg/kg meloxicam) was administered. A ~1.5 cm incision was made in the skin on the dorsal aspect of the head and neck and the neck muscles were carefully retracted. A small window was drilled into the ventral aspect of the interparietal bone, and the head was positioned at a 5–10° ventral angle to visualize the DVC. Injections were performed using Hamilton Neuros syringes (Hamilton, 65460-02) and a Quintessential Stereotaxic Injector (Stoelting, 53311) using the following coordinates: ML: 0.3 mm, AP: −7.5 mm, DV: 4.3 mm. REV-ERBα/β were knocked out in the DVC of male *Nr1d1*$^{fl/fl}$/*Nr1d2*$^{fl/fl}$ mice via bilateral intraparenchymal injection of 50 nL of 5×10^7 GC of AAV8-CMV-Cre (Addgene, 105538-AAV8) to create DVC RDKO. For the control group, *Nr1d1*$^{fl/fl}$/*Nr1d2*$^{fl/fl}$ mice received bilateral injections of the same volume and titer of AAV8-CMV-EGFP (Addgene, 105530-AAV8). Needles remained in both injection sites for ~30 s to ensure penetrance of the injection and prevent backflow. After needles were removed from the second injection, neck muscles were repositioned, and skin was sutured with absorbable thread. Post-operative analgesic (bupivacaine) was administered to the skin around the incision site. Animals were then placed in a clean, warmed cage for recovery and were maintained at 30 °C for three days post-op with soft diet and water gel (ClearH_2O, 72-06-5022 and 70-01-5002 respectively) to supplement *ad libitum* NCD and water. Animals were given subcutaneous 5 mg/kg meloxicam for three days post-op and were weighed and monitored for ten days post-op. To allow for sufficient surgical recovery and viral expression, animals were maintained on *ad libitum* NCD and water for 2–4 weeks post-op before metabolic phenotyping or beginning HFD.

2.3. Metabolic rate measurement

Metabolic rate was determined by *in vivo* indirect calorimetry in Comprehensive Lab Animal Monitoring System (CLAMS, Columbus Instruments) cages. Animals were placed singly in CLAMS cages with bedding, food, and water that mimicked the home cage environment. After two days of adaptation, experimental data were collected for three days. Data were acquired every 15 min by Oxymax software.

2.4. Food intake measurement

Food intake was measured by Biological Data Acquisition (BioDAQ, Research Diets) cages. Animals were placed singly in BioDAQ cages with bedding, food, and water that mimicked the home cage environment. After two days of acclimation, experimental data were collected for three consecutive days. Data were acquired at each food hopper interaction and analyzed by BioDAQ Data Analysis software. An average of the three consecutive days was determined for each animal and then summed over the light cycle, dark cycle, and total 24 h.

2.5. RNA extraction, cDNA synthesis, and RTqPCR

For DVC RNA extraction, the area was microdissected from the brainstem and homogenized with 1 mL of QIAzol Lysis Reagent (Qiagen, 79306) using Pellet-Pestel (Kimble, 749540). Intrascapular BAT and inguinal white adipose tissue (iWAT) was homogenized in 500uL of QIAzol Lysis Reagent using a TissueLyser system (Qiagen, 85300). After homogenization, total RNA from both tissues was purified and collected using RNeasy Mini Kits (Qiagen, 74004). RNA quality and quantity was determined by NanoDrop (Thermo Scientific, ND-ONE-W). cDNA was synthesized using High-Capacity cDNA Reverse Transcription kit (Applied Biosystems, 4368814). qPCR was run using Power SYBR Green PCR Master Mix (Applied Biosystems, 4368577) and QuantStudio 6 Flex Real-Time PCR system and software (Applied Biosystems, 4485691). All primers (Appendix) were validated, and qPCR results were analyzed by standard curve and normalization to *18s*.

2.6. RNAscope

For quantification of *Nr1d1* in the DVC, brains were rapidly removed and fixed overnight in 4% paraformaldehyde at 4C. Brains were then washed 3× with 0.1M phosphate-buffered saline (PBS, pH 7.4) and transferred to 30% sucrose in 0.1M PBS and maintained at 4C until the brains sunk. Brains were then embedded in OCT compound, frozen at −80C, and then sectioned on a cryostat in the coronal plane at 14 μm thickness. Slices were collected on Superfrost Plus slides (VWR) and stored at −80C until further analysis. RNAscope was performed as previously described [28]. Briefly, RNAscope Multiplex Fluorescent Reagent Kit v2 (ACDBio, 323110) was used per the manufacturer's instructions. Detection was carried out using a custom probe produced by ACDBio for *Nr1d1* mRNA targeting exons 4 and 5 (Mm-Nr1d1-O2-C3, 1097521-C3). Following a series of amplification steps, sections were mounted with VECTASHIELD PLUS with DAPI (Vector Labs, H-2000). Slides were imaged on an EVOS FL Auto 2 (Thermo Scientific, AMAFD2000) widefield microscope at 10× magnification. Images provided are representative views of control and DVC RDKO sections to confirm lack of robust *Nr1d1* expression within the DVC of the RDKO group.

2.7. Brown adipose tissue histology and immunofluorescence

Freshly isolated BAT was fixed overnight in 4% paraformaldehyde at 4 °C before EtOH dehydration. Tissue was embedded in paraffin and sectioned at 7 μm. Hematoxylin and eosin (H&E) staining and immunofluorescence (IF) for tyrosine hydroxylase (TH) was performed by the Institute of Diabetes, Obesity, and Metabolism Histology Core using a standard protocol. The antibody for TH staining was obtained from EMD Millipore (AB1542). Slides were imaged on an EVOS FL Auto 2 (Thermo Scientific, AMAFD2000) widefield microscope.

Histological slides were imaged at 20× magnification and IF was imaged at 40× magnification. Cell number and size in histology samples and IF signal were analyzed using FIJI Is Just ImageJ (FIJI, NIH).

2.8. Statistical analysis

Statistical analysis and graphing were performed using GraphPad Prism 7 software. All data were presented as mean ± standard error measurement (SEM) and statistical significance was set *a priori* as $p < 0.05$. Gene expression, final body weight, food intake, and brown adipocyte histology and IF were compared using the Mann–Whitney U-test. Running body weight gain, metabolic rate, and activity were compared using a repeated measures analysis of variance (RM ANOVA) with a Tukey post-hoc test. Correlation analyses were performed using Pearson correlation analysis.

3. RESULTS AND DISCUSSION

3.1. REV-ERBα/β double knockout in the dorsal vagal complex (DVC RDKO)

Male *Nr1d1*$^{fl/fl}$/*Nr1d2*$^{fl/fl}$ mice received stereotaxic injections of AAV8-CMV-EGFP or AAV8 CMV-Cre to create the control and DVC RDKO groups, respectively. After viral expression and metabolic phenotyping, the DVC was microdissected from the hindbrain for RTqPCR confirmation of the knockout (Figure 1A). REV-ERBα (*Nr1d1*) and REV-ERBβ (*Nr1d2*) exhibited reduced expression in the DVC of DVC RDKO animals (Figures 1B). REV-ERBα/β are constitutive repressors of the circadian clock activator, *Arntl* (BMAL1) and the accessory circadian clock repressor, *Nfil3* (E4BP4) [17]. Consistent with reduced expression of their repressors, *Arntl* and *Nfil3* expression were increased in DVC RDKO animals (Figure 1C). *In situ Nr1d1* expression was found to be decreased throughout the DVC (Figure 1D).

3.2. DVC RDKO does not impact food intake or body weight on normal chow diet (NCD)

The DVC is a major regulatory site for food intake, satiety, and energy balance [5]. Therefore, we hypothesized DVC RDKO would result in altered food intake and affect body weight. However, DVC RDKO animals maintained on NCD did not exhibit different food intake when analyzed over 24 h (Figure 2A). DVC RDKO also did not exhibit increased body weight (Figure 2B).

3.3. DVC RDKO exacerbates diet-induced obesity and dampens metabolic activity

We have previously shown that RDKO in the hypothalamus does not manifest in a metabolic phenotype on NCD [28]. We therefore hypothesized that a metabolic stressor, such as an obesogenic HFD, is necessary to uncover the metabolic deregulatory effects of DVC RDKO. To explore this possibility, control and DVC RDKO mice were placed on a 60% HFD for 12 weeks. We observed increased weight gain in DVC RDKO mice (Figure 3A). The DVC RDKO animals exhibited similar meal size, eating frequency, and time spent eating (Supplementary Figure 1A-E), but displayed a non-significant increase in grams of food consumed (Figure 3B) and kcal of food consumed (Supplementary Figure 1F) as compared to HFD-fed controls. We also observed decreased VO_2 in the DVC RDKO animals (Figure 3C) with a negative correlation to body weight when fit to the entire model (Supplementary Figure 2A), but no correlation to body weight when fit to the control or

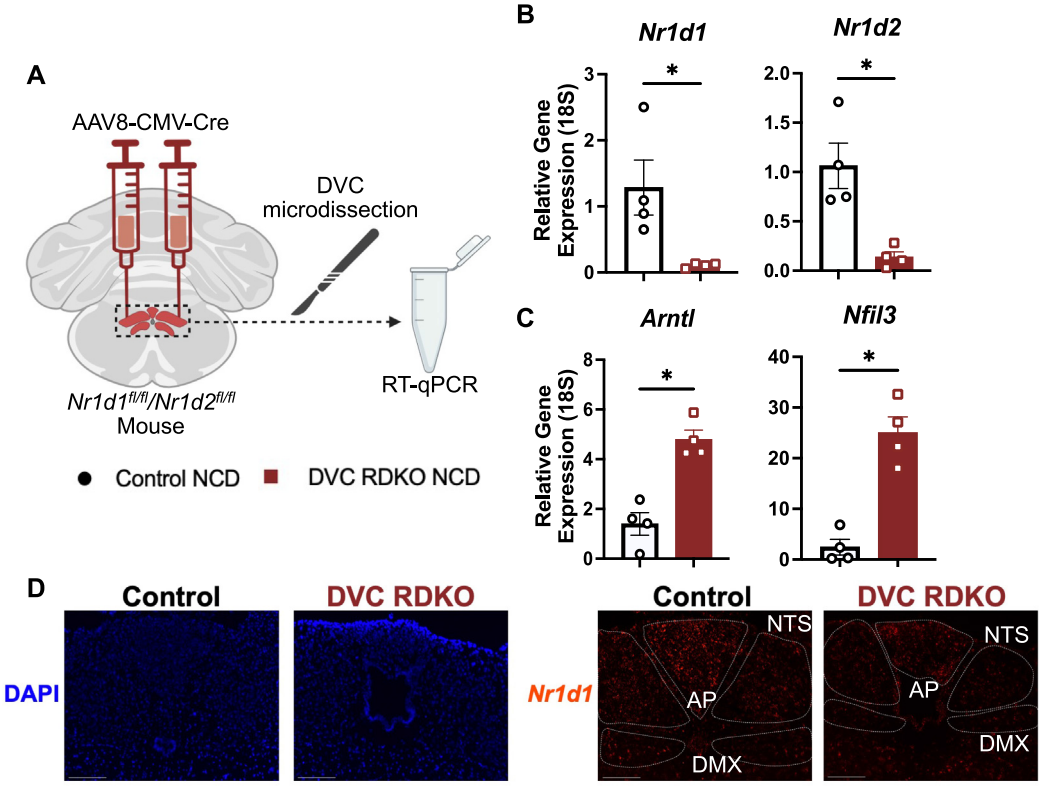

Figure 1: REV-ERBα/β double knockout in the dorsal vagal complex (DVC RDKO). A) Experimental scheme for DVC RDKO generation and tissue processing. **B–C)** RT-qPCR analysis of *Nr1d1* (REV-ERBα), *Nr1d2* (REV-ERBβ), *Arntl* (BMAL1), and *Nfil3* (E4BP4) ($n = 4–5$, mean ± SEM). **D)** Representative images at 10× magnification from RNAscope of Control and DVC RDKO animals for confirmation of *Nr1d1* knockout in the DVC (scale bar 275 μm). **B–C)** Results were compared by Mann–Whitney U-test. $*p < 0.05$, $**p < 0.01$, $***p < 0.001$.

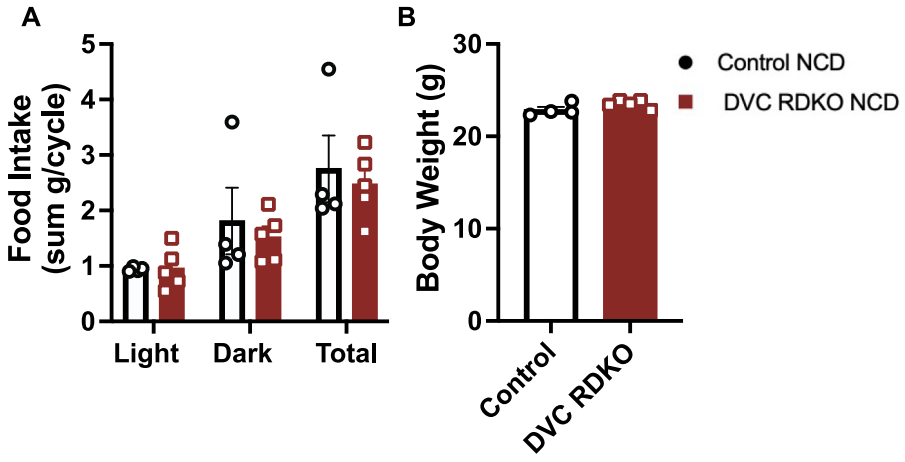

Figure 2: DVC RDKO does not impact food intake or body weight on normal chow diet (NCD). A) Light cycle, dark cycle, and total 24hr food intake measurements ($n = 4–5$, mean ± SEM). **B)** Final body weight measurement 5–7 weeks after stereotaxic injection for Control and DVC RDKO animals on NCD ($n = 4–5$, mean ± SEM). Data was analyzed by Mann–Whitney U-test.

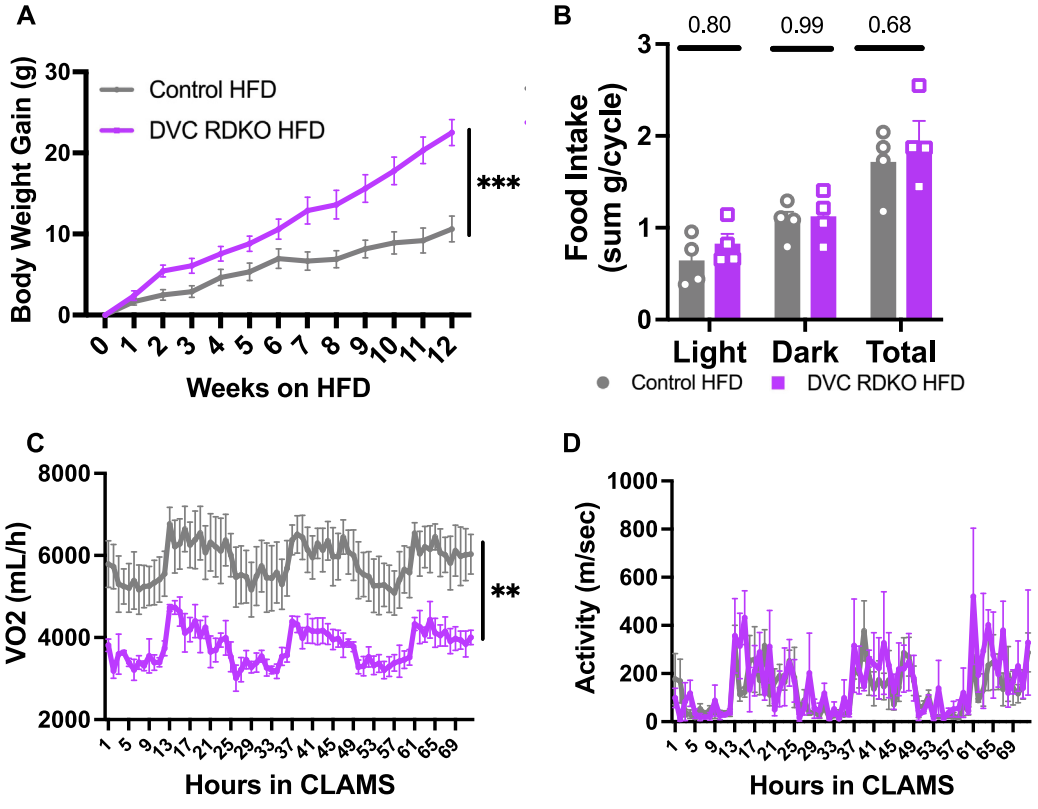

Figure 3: DVC RDKO exacerbates diet-induced obesity and dampens metabolic activity. A) Running body weight gain graph for 12 weeks of HFD ($n = 4–5$, mean ± SEM). **B)** Light, dark, and total food intake on HFD ($n = 3–4$, mean ± SEM). **C)** Oxygen consumption as a measure for metabolic rate on HFD ($n = 3–4$, mean ± SEM). **D)** Activity measurements on HFD ($n = 3–4$, mean ± SEM). **A&C)** Results were compared by repeated measures ANOVA. **B)** Results were compared by Mann–Whitney U-test. $^{**}p < 0.01$, $^{***}p < 0.001$.

DVC RDKO groups independently (control: r = −0.542, $p = 0.635$; DVC RDKO: r = 0.986, $p = 0.1071$). This change was not accompanied with altered locomotor activity (Figure 3D). We conclude that a minor increase in food intake coupled with decreased VO_2 over the course of HFD exposure exacerbated the DIO phenotype in DVC RDKO.

3.4. DVC RDKO decreases molecular signatures for brown adipose tissue (BAT) activity

Since decreased VO_2 in the DVC RDKO animals occurred independent of changes in locomotor activity, we explored other sources affecting the phenotype. Brown adipose tissue (BAT) quickly oxidizes lipid stores

to regulate metabolic rate and its activity is regulated by outflow from the sympathetic nervous system (SNS) [30].

The BAT of DVC RDKO animals had large, unilocular adipocytes compared to the control group (Figure 4A) and was consistent with increased size by quantification (Figure 4B). Gene markers for BAT activity *Ppargc1a, Ucp1, Prdm16,* and *Cidea* were decreased in the DVC RDKO group (Figure 4C) with a negative correlation between the relative expression of these genes and grams of body weight gained on HFD (Figure 4D). Changes in BAT gene expression were not observed on NCD suggesting a synergistic effect of DVC RDKO and HFD feeding on BAT pathophysiology (Supplementary Figure 3A).

Due to REV-ERBs' role as repressors of the circadian clock, DVC RDKO may also induce exacerbated weight gain due to desynchrony among the DVC, the rest of the body, and the external environment. Indeed, the DVC has been shown to have a robust cell-autonomous clock that can be altered by HFD feeding [31–33]. However, this possibility requires further study.

3.5. DVC RDKO decreases calcitonin receptor gene expression in the DVC and tyrosine hydroxylase expression in the BAT

There are established connections between the DVC and BAT [34,35]. Specifically, the NTS of the DVC projects to thalamic regions that regulate activity in the pre-sympathetic dorsal raphe nuclei (DRN) [35]. Through these neural networks, the DVC can modulate BAT activity in response to the humoral and neural feeding signals it receives from the periphery [36–38]. Of the several factors and receptors that mediate DVC control of energy balance, we measured gene expression for *Gcg* (glucagon-like peptide), *Insr* (insulin receptor), *Lepr* (leptin receptor), and *Calcr* (calcitonin receptor) from microdissected DVCs in control and DVC RDKO animals fed HFD. *Gcg* and *Insr* exhibited a non-significant decrease in expression, but *Calcr* was significantly decreased (Figure 5A). Direct REV-ERBα/β targets exhibit overexpression upon RDKO due to release from REV-ERB repressive activity. The mechanism underlying decreases in *Gcg, Insr,* and *Calcr* following RDKO is less clear, but most likely due to loss of REV-ERB repression of direct regulators of these genes. Indeed, in several other tissues including liver and heart, loss of REV-ERBs increases the expression of *Nfil3* (E4BP4), a powerful transcriptional repressor whose target genes thus become further repressed in the absence of REV-ERBs [39,40].

The decrease in *Calcr* (CTR) gene expression was intriguing because CTRs are G-protein coupled receptors that are often found in complex with a receptor activating modifying protein (RAMP) to form the heterodimerized amylin receptor [41]. Activation of CTRs in the DVC has been found to regulate not only food intake, but energy expenditure through indirect NTS projections to the DRN that modulate SNS-stimulated BAT activity [36–38,42,43]. Therefore, we measured BAT expression of tyrosine hydroxylase (*Th*) to determine disruptions in general SNS outflow and found that *Th* RNA and TH protein expression were decreased in the DVC RDKO animals (Figure 5B–D). *Th* was also decreased in inguinal white adipose tissue (iWAT) suggesting that DVC RDKO non-specifically dampens SNS tone under HFD-fed conditions (Supplementary Figure 4A-B). Although full elucidation of this mechanism requires additional testing, our data suggests that DVC RDKO may increase sensitivity to HFD by dampening SNS outflow.

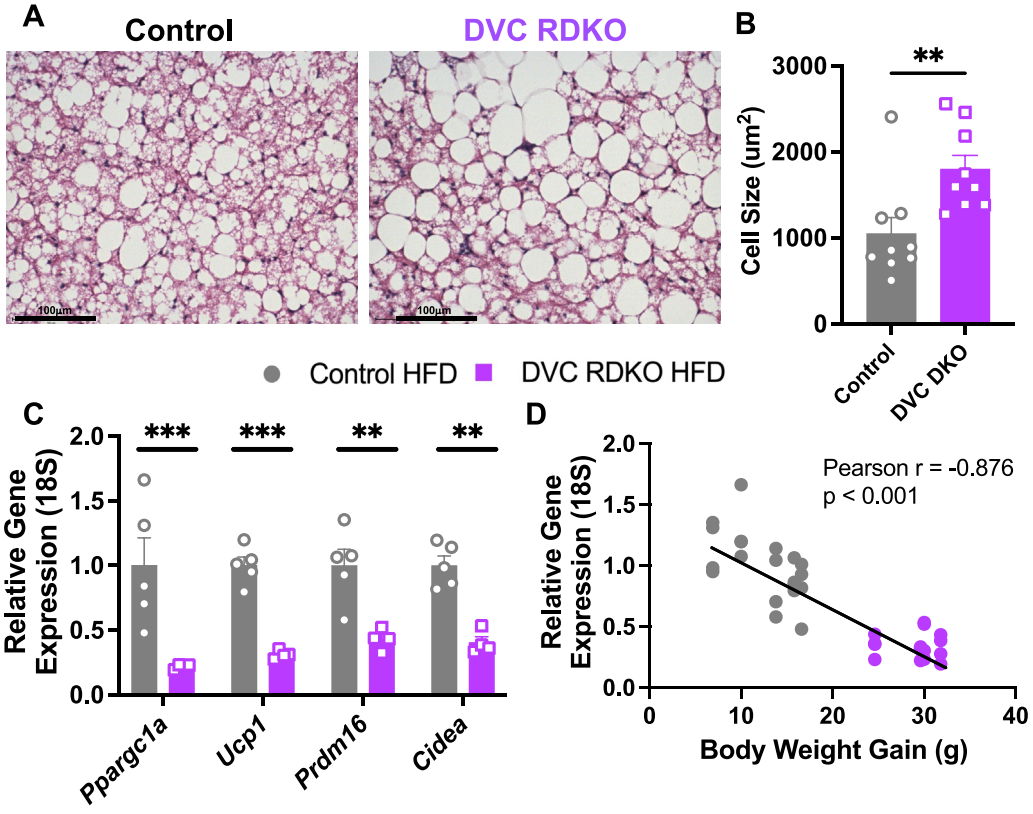

Figure 4: DVC RDKO decreases molecular signatures for BAT activity on HFD. A) Representative images of BAT from control and DVC RDKO animals after 12 weeks of 60% HFD feeding. **B)** Quantification of BAT adipocyte size from 3 technical replicates of 3 biological replicates ($n = 9$, mean ± SEM). **C-D)** RTqPCR for BAT activity markers (**C**) and correlation of their expression with body weight gain at week 12 (**D**) ($n = 4$–5, mean ± SEM). **B–C)** Results were compared by Mann–Whitney U-test. **D)** Results were analyzed by Pearson correlation. $^{**}p < 0.01$, $^{***}p < 0.001$.

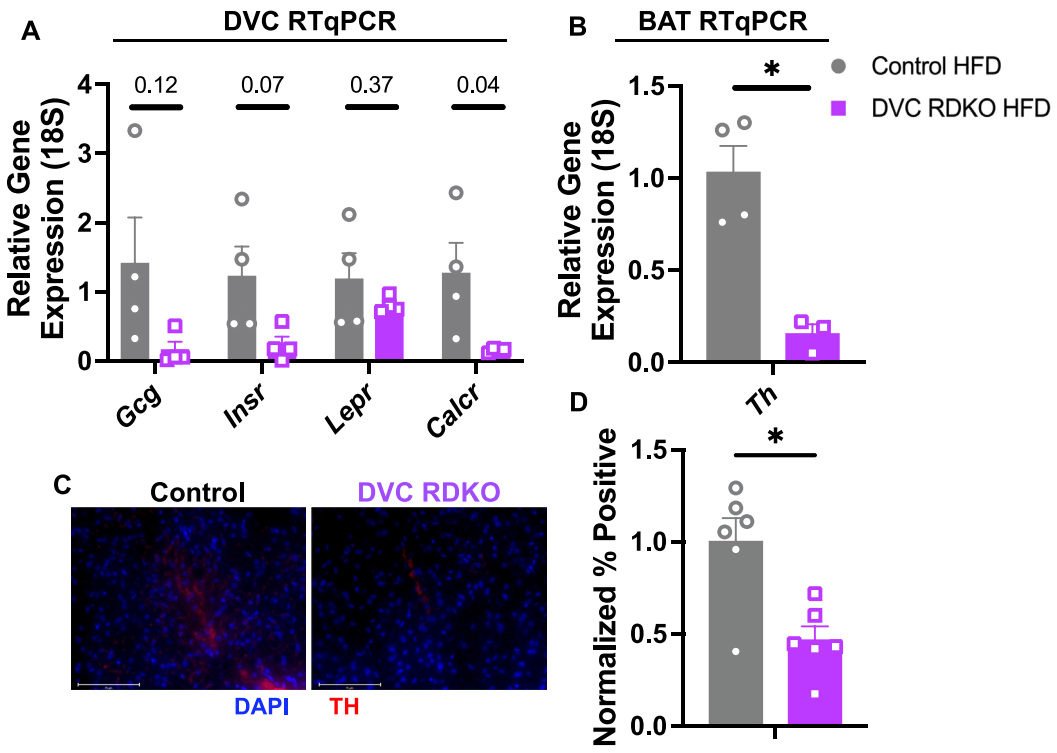

Figure 5: DVC RDKO decreases markers of sympathetic outflow to the BAT. A) DVC RTqPCR for gene markers of energy balance regulation ($n = 4$, mean ± SEM). **B)** BAT RTqPCR for *Th* ($n = 3$–4, mean ± SEM). **C)** Representative images at 40× magnification of IF for DAPI and TH from Control and DVC RDKO BAT (scale bar 75 μm). **D)** Quantification of fluorescent signal in six images per group from three biological replicates ($n = 3$, mean ± SEM). **A,B,D)** Results were compared by Mann–Whitney U-test. $^{*}p < 0.05$, $^{**}p < 0.01$.

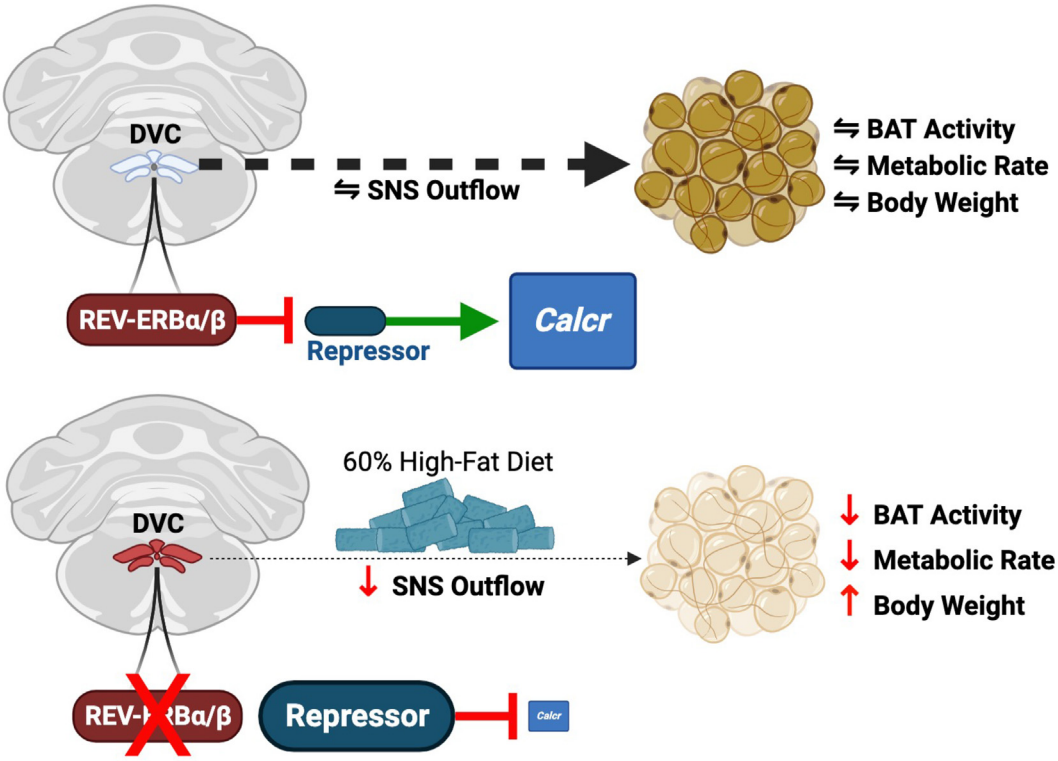

Figure 6: Proposed Model. REV-ERBα/β in the dorsal vagal complex (DVC) may indirectly regulate sympathetic nervous system (SNS) outflow to the brown adipose tissue (BAT) potentially by orchestrating calcitonin receptor (*Calcr*) gene expression. Upon feeding with a 60% high-fat diet, DVC REV-ERBα/β double knockout (DVC RDKO) induced a remarkable exacerbation of diet-induced obesity due to decreased basal metabolic rate and markers for BAT activity. We postulate that this was potentially caused by de-repression of repressors for *Calcr* in the DVC that indirectly decrease SNS outflow to the BAT.

4. CONCLUSIONS

DVC RDKO exacerbated DIO due to decreased basal metabolic rate and markers for BAT activity. We postulate that this was caused by de-repression of repressors for the key energy balance regulators in the DVC (Figure 6). This was accompanied by diminished *Th* expression in the BAT suggesting decreased activity of the SNS (Figure 6). Definitive characterization of CTR in the DVC as a potential mechanism for the DVC RDKO phenotype requires further testing. Follow up studies utilizing next-generation sequencing techniques and rescue studies should be performed to determine whether other signaling pathways are impacted by DVC RDKO. Furthermore, we used a CMV promoter to drive Cre expression thereby deleting REV-ERBs in all cell types. It is unknown how specific cell types within the DVC function to affect DIO, energy expenditure, and BAT activity in our model, and it should be pointed out that all experiments were performed at 22 °C, which is a thermal stressor for mice. As obesity and metabolic disease become increasingly prevalent in Western society, it is crucial to understand the central mechanisms that underlie energy homeostasis. Herein, we uncovered a role for the REV-ERBα/β nuclear receptors in the DVC for maintaining energy balance and metabolic rate potentially through indirect, calcitonin-mediated sympathetic outflow to the BAT in a mouse model.

AUTHOR CONTRIBUTIONS

LNW and MAL designed the study, interpreted the data, and edited the manuscripts. LNW and SMF performed survival surgeries. LNW performed RTqPCR, statistical analysis, and prepared the manuscript. LNW, LCM, AJA, and CCC performed sacrifice and tissue collection. LNW, LCM, and AJA performed metabolic phenotyping and food intake experiments. MB performed RNAscope experiments. LCM performed breeding and genotyping of *Nr1d1*$^{fl/fl}$/*Nr1d2*$^{fl/fl}$ mice. LNW and SMF designed and optimized surgical procedure for DVC injection. LNW, MRH, and MAL designed studies and interpreted gene expression data in the BAT and DVC. All authors reviewed and edited the manuscript.

ACKNOWLEDGEMENTS

The authors would like to thank B. Krusen and T. Acavedo for their invaluable help and discussion. We thank L. Cheng from the Penn Institute for Diabetes, Obesity, and Metabolism Histology core, and the Rodent Metabolic Phenotyping Core of the Penn Diabetes Research Center (P30DK19525). Multiple figures in this manuscript (Figures 1A and 6) were made using BioRender. This work was supported by NIH R01DK45596 (MAL), NIH F32DK128984 (LNW), NIH T32DK007314 (LNW), NIH R25MH119043 (CCC), NIH R01DK105155 and the JPB Foundation (MAL).

DECLARATION OF COMPETING INTEREST

The authors declare the following competing interests:
MAL is on the advisory board and has received research funding from Pfizer and is on the advisory board and is co-founder of Flare Therapeutics. MRH receives additional research funding from Boehringer Ingelheim, Novo Nordisk, Pfizer, Gila Therapeutics, and Eli Lilly & Co. that was not used in support of these studies. AJA, CCC, LNW, LCM, MB, and SMF have no competing interests to declare.

DATA AVAILABILITY

Data will be made available on request.

APPENDIX A. SUPPLEMENTARY DATA

Supplementary data to this article can be found online at https://doi.org/10.1016/j.molmet.2023.101861.

APPENDIX

RTqPCR Primers

	Forward (5' -> 3')	Reverse (5' -> 3')
Nr1d1	GTCTCTCCGTTGGCATGTCT	CCAAGTTCATGGCGCTCT
Nr1d2	CGGATCACATGGTCGAGGAG	TGCTCCTCCGAAAGAAACCC
Arntl	CTTTATCAGCTGCACATCACTCAGA	GGACATTGCATTGCATGTTGG
Nfil3	GCTCTTTTGTGGACGAGCAT	ACCGAGGACACCTCTGACAC
Ppargc1a	GGACATGTGCAGCCAAGACTCT	CACTTCAATCCACCCAGAAAGCT
Ucp1	GGCCAGTTGGTTTTCACAGA	GGATTGGCCTCTACGACTCA
Prdm16	CAGCACGGTGAAGCCATT	CGCGTGCATCCGCTTGTG
Cidea	TGCTCTTCTGTATCGCCCAGT	GCCGTGTTAAGGAATCTGCTG
Gcg	CCTTCAAGACACAGAGGAGAACC	CTGTAGTCGCTGGTGAATGTGC
Insr	AGATGAGAGGTGCAGTGTGGCT	GGTTCCTTTGGCTCTTGCCACA
Lepr	CTTTCCTGTGGACAGAACCAGC	AGCACTGAGTGACTCCACAGCA
Calcr	AAGATGGACCCTCATGCCAGTG	CTCGTCGGTAAACACAGCCATG
Th	TGCACACAGTACATCCGTCATGC	GCAAATGTGCGGTCAGCCAACA
18s	AGTCCCTGCCCTTTGTACACA	CGATCCGAGGGCCTCACTA

REFERENCES

[1] Aronne LJ, Hall KD, Jakicic JM, Leibel RL, Lowe MR, Rosenbaum M, Klein S. Describing the Weight-reduced State: Physiology, Behavior, and Interventions. Obesity 2021;29:S9–24. https://doi.org/10.1002/oby.23086. Wiley Online Libr.

[2] Schwartz MW, Seeley RJ, Zeltser LM, Drewnowski A, Ravussin E, Redman LM, Leibel RL. Obesity Pathogenesis: An Endocrine Society Scientific Statement. Endocrine Rev 2017. https://doi.org/10.1210/er.2017-00111. academic.oup.com.

[3] Hall KD, Farooqi IS, Friedman JM, Klein S, Loos RJF, Mangelsdorf DJ, et al. The energy balance model of obesity: beyond calories in, calories out. Am J Clin Nutr 2022;115:1243–54. https://doi.org/10.1093/AJCN/NQAC031.

[4] Spiegelman BM, Flier JS. Obesity and the regulation of energy balance. Cell 2001;104:531–43. https://doi.org/10.1016/S0092-8674(01)00240-9.

[5] Grill HJ, Hayes MR. Hindbrain neurons as an essential hub in the neuroanatomically distributed control of energy balance. Cell Metabol 2012;16:296–309. https://doi.org/10.1016/j.cmet.2012.06.015.

[6] Grill HJ, Kaplan JM. The neuroanatomical Axis for control of energy balance. Front Neuroendocrinol 2002;23:2–40. https://doi.org/10.1006/frne.2001.0224.

[7] Ludwig MQ, Cheng W, Gordian D, Lee J, Paulsen SJ, Hansen SN, et al. A genetic map of the mouse dorsal vagal complex and its role in obesity. Nat Metab 2021;3:530–45. https://doi.org/10.1038/s42255-021-00363-1. 2021 34.

[8] Berthoud HR, Albaugh VL, Neuhuber WL. Gut-brain communication and obesity: understanding functions of the vagus nerve. J Clin Invest 2021:131. https://doi.org/10.1172/JCI143770.

[9] McDougle M, Araujo A de, Vergara M, Singh A, Yang M, Braga I, et al. de Fats and sugars recruit distinct gut-brain circuits to control food intake and reward. Faseb J 2022:36. https://doi.org/10.1096/FASEBJ.2022.36.S1.00R29.

[10] Berthoud HR. The vagus nerve, food intake and obesity. Regul Pept 2008;149:15–25. https://doi.org/10.1016/J.REGPEP.2007.08.024.

[11] Laughton WB, Powley TL. Localization of Efferent Function in the Dorsal Motor Nucleus of the Vagus. 1987. p. 252. https://doi.org/10.1152/AJPREGU.1987.252.1.R13.

[12] Stein LM, Lhamo R, Cao A, Workinger J, Tinsley I, Doyle RP, et al. Dorsal vagal complex and hypothalamic glia differentially respond to leptin and energy balance dysregulation. Transl Psychiatry 2020;10:1—12. https://doi.org/10.1038/s41398-020-0767-0.

[13] Cheng W, Ndoka E, Hutch C, Roelofs K, MacKinnon A, Khoury B, et al. Leptin receptor-expressing nucleus tractus solitarius neurons suppress food intake independently of GLP1 in mice. JCI insight 2020;5. https://doi.org/10.1172/JCI.INSIGHT.134359.

[14] Berglund ED, Liu T, Kong X, Sohn JW, Vong L, Deng Z, et al. Melanocortin 4 receptors in autonomic neurons regulate thermogenesis and glycemia. Nat Neurosci 2014;17:911—3. https://doi.org/10.1038/nn.3737. 2014 177.

[15] Filippi BM, Bassiri A, Abraham MA, Duca FA, Yue JTYY, Lam TKT. Insulin signals through the dorsal vagal complex to regulate energy balance. Diabetes 2014;63:892—9. https://doi.org/10.2337/DB13-1044.

[16] Stein LM, McGrath LE, Lhamo R, Koch-Laskowski K, Fortin SM, Skarbaliene J, et al. The long-acting amylin/calcitonin receptor agonist ZP5461 suppresses food intake and body weight in male rats. Am J Physiol Regul Integr Comp Physiol 2021;321:R250—9. https://doi.org/10.1152/AJPREGU.00337.2020/ASSET/IMAGES/LARGE/AJPREGU.00337.2020_F006.JPEG.

[17] Adlanmerini M, Lazar MA. The REV-ERB nuclear receptors: timekeepers for the core clock period and metabolism. Endocrinology 2023:164. https://doi.org/10.1210/ENDOCR/BQAD069.

[18] Cho H, Zhao X, Hatori M, Yu RT, Barish GD, Lam MT, et al. Regulation of circadian behaviour and metabolism by REV-ERB-a and REV-ERB-B. 2012. https://doi.org/10.1038/nature11048.

[19] Feng D, Liu T, Sun Z, Bugge A, Mullican SE, Alenghat T, et al. A circadian rhythm orchestrated by histone deacetylase 3 controls hepatic lipid metabolism. Science 2011;331:1315—9. https://doi.org/10.1126/SCIENCE.1198125.

[20] Zhang Y, Fang B, Emmett MJ, Damle M, Sun Z, Feng D, et al. GENE REGULATION. Discrete functions of nuclear receptor rev-erbα couple metabolism to the clock. Science 2015;348:1488—92. https://doi.org/10.1126/science.aab3021.

[21] Bugge A, Feng D, Everett LJ, Briggs ER, Mullican SE, Wang F, et al. Rev-erbα and rev-erbβ coordinately protect the circadian clock and normal metabolic function. Genes Dev 2012;26:657—67. https://doi.org/10.1101/gad.186858.112.

[22] Guan D, Xiong Y, Trinh TM, Xiao Y, Hu W, Jiang C, et al. The hepatocyte clock and feeding control chronophysiology of multiple liver cell types downloaded from. Science 2020;369:1388—94.

[23] Ding G, Li X, Hou X, Zhou W, Gong Y, Liu F, et al. Corrections & amendments author correction: REV-ERB in GABAergic neurons controls diurnal hepatic insulin sensitivity check for updates 2021;595. https://doi.org/10.1038/s41586-021-03654-5.

[24] Mang GM, La Spada F, Emmenegger Y, Chappuis S, Ripperger JA, Albrecht U, et al. Altered sleep homeostasis in rev-erbα knockout mice. Sleep 2016;39:589—601. https://doi.org/10.5665/SLEEP.5534.

[25] Jager J, Timothy O'Brien W, Manlove J, Krizman EN, Fang B, Gerhart-Hines Z, et al. Behavioral changes and dopaminergic dysregulation in mice lacking the nuclear receptor rev-erbα. Mol Endocrinol 2014;28:490—8. https://doi.org/10.1210/ME.2013-1351.

[26] Cho H, Zhao X, Hatori M, Yu RT, Barish GD, Lam MT, et al. Regulation of circadian behavior and metabolism by rev-erbα and rev-erbβ. Nature 2012;485:123. https://doi.org/10.1038/NATURE11048.

[27] Adlanmerini M, Krusen BM, Nguyen HCB, Teng CW, Woodie LN, Tackenberg MC, et al. REV-ERB nuclear receptors in the suprachiasmatic nucleus control circadian period and restrict diet-induced obesity. Sci Adv 2021;7. https://doi.org/10.1126/SCIADV.ABH2007/SUPPL_FILE/SCIADV.ABH2007_TABLE_S2.ZIP.

[28] Adlanmerini M, Nguyen HCB, Krusen BM, Teng CW, Geisler CE, Peed LC, et al. Hypothalamic REV-ERB nuclear receptors control diurnal food intake and leptin sensitivity in diet-induced obese mice. J Clin Invest 2021:131. https://doi.org/10.1172/JCI140424.

[29] Dierickx P, Emmett MJ, Jiang C, Uehara K, Liu M, Adlanmerini M, et al. SR9009 has REV-ERB—independent effects on cell proliferation and metabolism. Proc Natl Acad Sci USA 2019;116:12147—52. https://doi.org/10.1073/pnas.1904226116.

[30] Cannon B, Nedergaard J. Brown adipose tissue: function and physiological significance. Physiol Rev 2004;84:277—359. https://doi.org/10.1152/PHYSREV.00015.2003/ASSET/IMAGES/LARGE/Z9J0010402890022.JPEG.

[31] Chrobok L, Klich JD, Jeczmien-Lazur JS, Pradel K, Palus-Chramiec K, Sanetra AM, et al. Daily changes in neuronal activities of the dorsal motor nucleus of the vagus under standard and high-fat diet. J Physiol 2022;600:733—49. https://doi.org/10.1113/JP281596.

[32] Chrobok L, Klich JD, Sanetra AM, Jeczmien-Lazur JS, Pradel K, Palus-Chramiec K, et al. Rhythmic neuronal activities of the rat nucleus of the solitary tract are impaired by high-fat diet — implications for daily control of satiety. J Physiol 2022;600:751—67. https://doi.org/10.1113/JP281838.

[33] Chrobok L, Northeast RC, Myung J, Cunningham PS, Petit C, Piggins HD. Timekeeping in the hindbrain: a multi-oscillatory circadian centre in the mouse dorsal vagal complex. Commun Biol 2020;3:1—12. https://doi.org/10.1038/s42003-020-0960-y.

[34] Holland J, Sorrell J, Yates E, Smith K, Arbabi S, Arnold M, et al. A brain-melanocortin-vagus Axis mediates adipose tissue expansion independently of energy intake. Cell Rep 2019;27:2399—2410.e6. https://doi.org/10.1016/J.CELREP.2019.04.089.

[35] Cao WH, Madden CJ, Morrison SF. Inhibition of Brown adipose tissue thermogenesis by neurons in the ventrolateral medulla and in the nucleus tractus solitarius. Am J Physiol Regul Integr Comp Physiol 2010;299. https://doi.org/10.1152/AJPREGU.00039.2010.

[36] Skibicka KP, Grill HJ. Hindbrain leptin stimulation induces anorexia and hyperthermia mediated by hindbrain melanocortin receptors. Endocrinology 2009;150:1705. https://doi.org/10.1210/EN.2008-1316.

[37] Fozzato A, New LE, Griffiths JC, Patel B, Deuchars SA, Filippi BM. Manipulating mitochondrial dynamics in the NTS prevents diet-induced deficits in Brown fat morphology and glucose uptake. Life Sci 2023;328:121922. https://doi.org/10.1016/J.LFS.2023.121922.

[38] Skibicka KP, Grill HJ. Energetic responses are triggered by caudal brainstem melanocortin receptor stimulation and mediated by local sympathetic effector circuits. Endocrinology 2008;149:3605—16. https://doi.org/10.1210/EN.2007-1754.

[39] Dierickx P, Zhu K, Carpenter BJ, Jiang C, Vermunt MW, Xiao Y, et al. Circadian REV-ERBs repress E4bp4 to activate NAMPT-dependent NAD+ biosynthesis and sustain cardiac function. Nat. Cardiovasc. Res. 2022;1:45. https://doi.org/10.1038/S44161-021-00001-9.

[40] Fang B, Everett LJ, Jager J, Briggs E, Armour SM, Feng D, et al. Circadian enhancers coordinate multiple phases of rhythmic gene transcription in vivo. Cell 2014;159:1140—52. https://doi.org/10.1016/J.CELL.2014.10.022.

[41] Pondel M. Calcitonin and calcitonin receptors: bone and beyond. Int J Exp Pathol 2000;81:405—22. https://doi.org/10.1046/J.1365-2613.2000.00176.X.

[42] Zakariassen HL, John LM, Lutz TA. Central control of energy balance by amylin and calcitonin receptor agonists and their potential for treatment of metabolic diseases. Basic Clin Pharmacol Toxicol 2020;127:163—77. https://doi.org/10.1111/BCPT.13427.

[43] Fernandes-Santos C, Zhang Z, Morgan DA, Guo DF, Russo AF, Rahmouni K. Amylin acts in the central nervous system to increase sympathetic nerve activity. Endocrinology 2013;154:2481—8. https://doi.org/10.1210/EN.2012-2172.

